Biosensors and Bioelectronics 143 (2019) 111609

Contents lists available at ScienceDirect

Biosensors and Bioelectronics

journal homepage: www.elsevier.com/locate/bios

A triple-amplification differential pulse voltammetry for sensitive detection of DNA based on exonuclease III, strand displacement reaction and terminal deoxynucleotidyl transferase

Xinyi Huang[a], Wuceng Niu[a], Jiayi Wu[a], Yang Wang[a], Chaorui Li[b], Jingfu Qiu[b], Jianjiang Xue[a,*]

[a] Department of Clinical Laboratory, University-Town Hospital of Chongqing Medical University, Chongqing, 401331, PR China
[b] School of Public Health and Management, Chongqing Medical University, Chongqing, 400016, PR China

ARTICLE INFO

Keywords:
Exonuclease III
Terminal deoxynucleotidyl transferase
Hairpin DNA
Alkaline phosphatase
Electrochemical biosensor

ABSTRACT

In this research, a sensitive and specific electrochemical biosensor for DNA detection was constructed. The highly sensitivity of this biosensor is due to the exploitation of exonuclease III-assisted double recycling and toehold-mediated strand displacement recycling to achieve the target triple recycling amplification, thus generating a large amount of Y-shaped DNA structures. Combination with a terminal deoxynucleotidyl transferase (TDT)-mediated cascaded signal amplification strategy can catalyze the repetitive incorporation of biotin-dUTP to the 3'-OH of the Y-shaped DNA. Via biotin-streptavidin interaction, multiple streptavidin-alkaline phosphatases were conjugated to the surface of an Au electrode and generated a sharply increasing electrochemical signal in a 1-naphthyl phosphate (1-NP) solution. In this method, an impressive detection limit of 0.05 fM was obtained, presenting outstanding selectivity with a dynamic response scope between 0.1 fM and 1 nM. Thus, the designed biosensor opens an avenue for DNA detection in clinical molecular diagnostics, pathogen detection, gene therapy, food safety and environmental monitoring.

1. Introduction

As modern science and technology develop rapidly, molecular diagnosis has become an increasingly popular method because it not only is highly sensitive and selective but also offers a faster turnaround time (Chua et al., 2011). As DNA is an important biomarker, trace DNA detection is of great demand in clinical diagnosis, pathogen detection, gene therapy, and food safety as well as environmental monitoring (Huang et al., 2015; Li et al., 2008; Tadmor et al., 2011). During the last decades, considerable efforts have been channeled toward the construction of sensitive and specific strategies for DNA detection, such as polymerase chain reaction (PCR) (Woolley et al., 1996), southern blotting (Southern, 2006), and DNA microarrays (Hashsham et al., 2004).

However, these approaches suffer from complex detection procedures, cumbersome instrumentation and relatively low sensitivity (Ferrier et al., 2015); thus, an effective, facile, and economical method for the detection and analysis of trace DNA is urgently required.

Recently, electrochemical biosensors have found an important place in the detection of DNA due to their rapidness, simplicity, portability, low cost, ease of miniaturization and high sensitivity (Ahmed et al., 2014; Li et al., 2011; Zhang et al., 2014; Zhu et al., 2012). To attain a sensitive detection of DNA, many signal amplification strategies have been reportedly used in DNA detection, such as strand displacement amplification (SDA) (Zeng et al., 2018), hybridization chain reaction (HCR) (Zeng et al., 2019c; Zhou et al., 2018), catalytic hairpin assembly (CHA) (Zeng et al., 2018), rolling circle amplification (RCA) (Zhang et al., 2018), enzyme-assisted target recycling (EATR) (Zeng et al., 2019a, 2019b), loop-mediated isothermal amplification (LAMP) (Hsieh et al., 2012) and DNA walker-based amplification (Lv et al., 2018). In this research, a signal amplification method for sensitive DNA detection was developed. This strategy consists of three parts: exonuclease III-assisted target recycling, strand displacement reaction (SDR)-mediated target recycling and terminal deoxynucleotidyl transferase (TDT)-mediated cascaded signal amplification.

Enzyme-assisted target recycling (EATR) is a common signal amplification method widely used in electrochemical biosensors (Zeng et al., 2019a, 2019b). Superior to other enzyme-assisted amplification techniques, this strategy exploits exonuclease-III, which is a sequence-independent enzyme. The enzyme can catalyze stepwise mononucleotide hydrolysis from the 3'-OH terminus of double-stranded DNA when the substrates are recessed or blunt, and the 3'-terminus does not

* Corresponding author.
E-mail address: jianjiangxue@163.com (J. Xue).

https://doi.org/10.1016/j.bios.2019.111609
Received 26 June 2019; Received in revised form 14 August 2019; Accepted 17 August 2019
Available online 22 August 2019
0956-5663/

require any specific recognition site and presents lower activities on single-stranded DNA or duplex DNAs with a protruding 3'-terminus (Bi et al., 2012). Therefore, exonuclease III offers a more versatile platform for the sensitive detection of DNA.

In addition, for further improving the sensitivity of the biosensor, we have introduced strand displacement reaction (SDR) technology. SDR is a well-known methodology within the DNA nanotechnology field and has been previously demonstrated to be effective for isothermal DNA amplification (Yao et al., 2015). SDR utilizes the exchange mechanism of a short single-stranded overhanging DNA domain (toehold) for initiating the target-triggered assembly of metastable hairpin probes into complicated DNA nanostructures (Chen et al., 2015b; Zhang and Seelig, 2011), for example, dendritic nanostructures (Xuan et al., 2015), nanowires (Wang et al., 2017a), nanotubes (Zhang et al., 2013), G-quadruplexes (Mendoza et al., 2016), hydrogels (Fern and Schulman, 2018), and tetrahedra (Feng et al., 2017). The exchange mechanism occurs only when the toehold of the double-stranded DNA complex is displaced by an exterior intruding short single-stranded DNA with its binding to the toehold domain to initiate the DNA self-assembly process. This strand migration procedure can occur at ambient temperature with no requirement of enzymes or a thermal annealing step (Chen et al., 2016). Through application of the toehold-mediated SDR technology, the initiator DNA has been used as an actual catalyst to catalyze repeated cycles of the assembly reaction to generate massive DNA nanostructures, providing hundredfold catalytic signal amplification of the target DNA (Bi et al., 2016). In this work, SDR not only improves the sensitivity of the biosensor but also forms a Y-shaped branched structure to further carry out TDT-mediated amplification reactions.

The TDT-mediated cascaded signal amplification strategy is a signal extension strategy that has been used for target molecule determination (Chen et al., 2017a; Hu et al., 2015; Shen et al., 2015). Terminal deoxynucleotidyl transferase is a type of DNA polymerase that is template independent and able to catalyze the incorporation of multiple deoxyribonucleoside triphosphates (dNTPs) to extend the 3′-OH terminus of DNA, producing a tail of deoxyribonucleoside triphosphates (dNTPs) at the 3′-OH terminus and providing a new application of signal amplification (Shi et al., 2017). Unlike other DNA polymerases, TDT is template independent and has been widely employed to elongate the DNA within solution or to fabricate DNA nanostructures from a surface, which is referred to as surface-initiated enzymatic polymerization (SIEP) (Chen et al., 2017a; Wang et al., 2016). Considering the signal amplification capability and operation flexibility of TDT, it was conceived to offer a promising opportunity for tremendous enhancement of the analytical signals of targets to achieve highly sensitive detection considering that new nucleic acid 3′-OH termini can be created after the DNA reaction.

In this work, we designed five hairpin DNA: hairpin 1 (H1), hairpin 2 (H2), hairpin 3 (H3), hairpin 4 (H4), and hairpin 5 (H5). First, the target DNA opens hairpin 1, made up of a double-stranded DNA with blunt 3'-terminus, through exonuclease III-assisted target recycling, a great amount of trigger DNA 1 (T1) and trigger DNA 2 (T2) are produced, representing as cycle I and cycle II. T2 opens the hairpin DNA 3, subsequently triggering cycle III, which enables SDR-mediated target recycling and leaves many Y-shaped DNA nanostructures on the electrode. Then, TDT catalyzes the incorporation of multiple biotin-11-dUTPs to extend the 3′-OH terminus of Y-shaped DNA to generate two biotin-11-dUTP tails, via biotin-streptavidin interaction; multiple streptavidin-alkaline phosphatases are combined on the surface of Au electrode and produce a large electrochemical signal in a 1-naphthyl phosphate solution. This strategy might offer a new sensing platform for highly specific and sensitive DNA detection.

2. Experimental section

2.1. Reagents and chemicals

Reagents and chemicals adopted within this research are demonstrated in Supplementary Material S1.

2.2. Apparatus

Apparatus used in this research are provided in Supplementary Material S2.

2.3. Fabrication of biosensor

Prior to use, each solution of hairpin structure DNA was heated to 95 °C for 5 min and later slowly cooled to ambient temperature to form the stem-loop structure. Afterwards, the solution was stored at 4 °C until use. After the Au electrodes were cleaned thoroughly in the conventional way, the electrodes were rinsed completely with ultrapure water and dried at room temperature. The thiolated hairpin DNA (H5) was incubated in 10 mM TCEP buffer for an hour at ambient temperature to decrease the amount of disulfide bonds and then diluted to 0.5 μM before assembly on the Au electrode. Afterwards, 10 μL of 0.5 μM H5 was dropped on the prepared Au electrode surface and incubated at 4 °C overnight.

After a thorough rinsing with Tris buffer, the electrode was dipped in 1 mM MCH for 1 h at room temperature to obtain a well-aligned DNA monolayer and occupy the remaining bare region. After rinsing thoroughly with Tris buffer to remove the unbound capture probe, 10 μL 1% BSA (w/v) was dropped on the electrode surface at 37 °C for 30 min to block the nonspecific site, preventing DNA and enzyme nonspecific adsorption on the electrode surface. Simultaneously, 10 μL of different concentrations of target DNA, 3 μl of 1 μM H1, 3 μl of 4 μM H2, 2 μl of 20 U/μl exonuclease-III and 2 μL of 10 × exonuclease-III buffer were mixed together (the final volume was 20 μL) and reacted for 40 min at 37 °C. Then, 5 μL of 5 μM H3 and 5 μL of 5 μM H4 were added to the solution. After rinsing with the Tris-T buffer and Tris buffer, the Au electrode was immersed in the mixture solution and incubated for 80 min at 37 °C. Following a thorough sequential washing with Tris-T buffer and Tris buffer, 10 μL of extension solution containing 1 μL of 100 μM dUTP-biotin, 1 μL of 2.5 IU/μL TDT, 2 μL of 5 × TDT buffer, and 6 μL of ultrapure water was dropped onto the surface of the Au electrode and allowed to remain on the electrode for 80 min at 37 °C. After washing thoroughly with Tris-T buffer and Tris buffer, 10 μL of DEA buffer including 2.5 μg/mL ST-ALP solution was dropped onto the surface of the electrode and remained there for 30 min at 37 °C. After the electrode was washed thoroughly by DEA-T buffer and DEA buffer, the electrochemical signal was measured in DEA buffer with 1 mg/mL 1-NP substrate by DPV.

2.4. Electrochemical measurement

The EIS measurements were executed with parameters that included a frequency sweep range from 10^{-1}–10^{5} Hz and a 10 mV amplitude. The CV measurements were performed with a potential window between −0.2 and 0.6 V and a scan rate of 100 mV s^{-1}. The DPV measurements were carried out with the voltage within the range of −0.05–0.55 V, modulation amplitude of 0.07 V, modulation time of 0.05 s and interval time of 0.2 s. All measurements were obtained under ambient conditions at room temperature (25 ± 1 °C).

3. Results and discussion

3.1. Working mechanism of the biosensor

The principle of the cascade signal amplification strategy and the

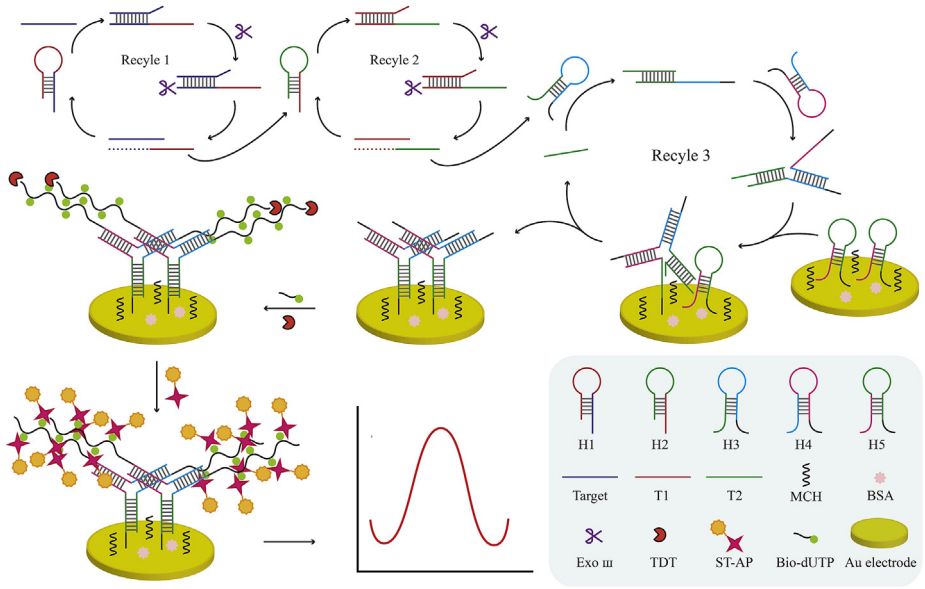

Scheme 1. Principle of the cascade signal amplification method and the working mechanism of the developed electrochemical biosensor for DNA determination.

working mechanism of the proposed electrochemical biosensor for DNA determination are illustrated in Scheme 1. We designed five hairpin DNA: hairpin 1 (H1), hairpin 2 (H2), hairpin 3 (H3), hairpin 4 (H4), and hairpin 5 (H5). For the purpose of avoiding the nucleic acid secondary structure and ensuring the desired hybridization events, the entire designed hairpin DNA was examined by Oligo Analyzer 3.1 (http://sg.idtdna.com/calc/analyzer) before use. All the hairpin DNA are duplex DNA with a 3'-overhang end over four bases long. Exonuclease III is not active on 3'-overhang ends of DNA that are more than four bases long (Wang et al., 2017b), so these hairpin DNA cannot be digested by exonuclease III. H1 includes two parts: one part is complementary to the target DNA from the 3'-terminus, and the other is complementary to part of H2. When target DNA exists, it hybridizes with H1 and unfolds H1 to form a DNA duplex with a blunt 3' -terminus. Therefore, Exo III is able to bind to the duplex region and stepwise hydrolyze the mononucleotides from the blunt 3'-terminus in the direction of 3' to 5', releasing the target DNA and the trigger DNA 1 (T1). The released target DNA continuously hybridizes with H1 and triggers the cleavage process (recycle I). The free trigger DNA 1 (T1) unfolds H2 through hybridization to form a DNA duplex that contains a blunt 3'-terminus. Therefore, Exo III is able to catalyze the stepwise hydrolysis of the mononucleotides from the blunt 3'-terminus, releasing both trigger DNA 2 (T2) and trigger DNA 1 (T1). Free trigger DNA 1 (T1) can take part in the following cycles of hybridization and cleavage procedures (recycle II) just as in cycle I. After many cycles, the enormous amount of trigger DNA 2 (T2) unfolds H3 through hybridization with H3 to form a DNA duplex with a 3'-overhang end over four bases long. Exo III cannot catalyze the stepwise hydrolysis of the mononucleotides from the overhang terminus to form an intermediate T2-H3. The opened region of H3 is complementary to H4 at the 3'-terminus, so the opened region of H3 opens H4 through hybridization with H4 to form the T2-H3-H4 complex and further hybridizes with the assembled H5 to form intermediate T2-H3-H4-H5 on the Au electrode surface. The intermediate T2-H3-H4-H5 is not stable and is likely to generate the Y-shaped DNA nanostructure (H3–H4–H5) by releasing initiator T2 (Chen et al., 2015a, 2016). The free T2 successively triggers the assembly of H3, H4 and H5 and thus generates numerous Y-shaped DNA nanostructures on the Au electrode surface, which dramatically amplify the signal of target DNA sequences (recycle III). Through triple recycling, countless Y-shaped DNA nanostructures assemble on the Au electrode surface. Afterwards, with the help of TDT, multiple biotin-11-dUTPs are incorporated to extend the 3′-OH terminus of Y-shaped DNA, consequently generating two biotin-11-dUTPs tails. Then, via biotin-streptavidin interaction, multiple streptavidin-alkaline phosphatases (ST-AP) are assembled on the surface of the Au electrode. Then, in the 1-naphthyl phosphate (1-NP) solution, ST-AP catalyzed the irreversible conversion of electrochemically inactive 1-NP to an electroactive phenol for producing an amplified electrochemical signal, which was quantified by DPV.

3.2. Characterization of electrode assembly process

To investigate the stepwise fabrication of the biosensor, EIS and CV measurements were employed to characterize each stage of sensor preparation. The EIS curves obtained by various modified electrodes are exhibited in Fig. 1A, the Randle modified equivalent circuit (inset in Fig. 1A) was used to fit the impedance spectroscopy and to determine electrical parameter values by using the ZSimpWin software. As exhibited in Fig. S1, the fitting curve showed good agreement with the measured data, indicating that this equivalent circuit was suitable for this electrochemical biosensor. The values of the equivalent circuit elements including the charge transfer resistance (Rct), the Warburg impedance (Zw), the Ohmic resistance of the electrolyte (Rs) and the constant phase element (CPE) are shown in Table S4. Rct reflects the electron transfer kinetics of the redox probe at the electrode surface; Rs dominates the electrolyte resistance between reference electrode and working electrode; Zw comes from the diffusion of ions from the bulk of the electrolyte to the interface; CPE represents a "leaking" and thus not ideal capacitor, which has a non-zero real component corresponding to energy dissipation. Very small changes were observed for the Rs values. CPE was a slight decreased, due to the immobilization of the oligonucleotides induced the sensor/electrolyte interface area smaller. Zw, which is related to the charge storage in the electrode, was also slightly decreased. This was due to the charge transfer process becomes more hindered by the DNA sequences immobilization on the electrode, and the load of intercalated charge within the oligonucleotides platform decreases consequently. The semicircle diameter of each EIS curve represents the charge transfer resistance (Rct) (Chen et al., 2017b). As exhibited in Fig. 1A, The bare Au electrode had a very small Rct value of about 330.6 Ω (curve a) in 10 mM $[Fe(CN)_6]^{3-/4-}$ solution, indicating a good charge transfer ability at the Au electrode surface. After H5 assembly on the bare electrode through Au–S interaction, the semicircle diameter increased (curve b) and the Rct value was about 986.3 Ω. This result was because the negatively charged phosphate backbone of the

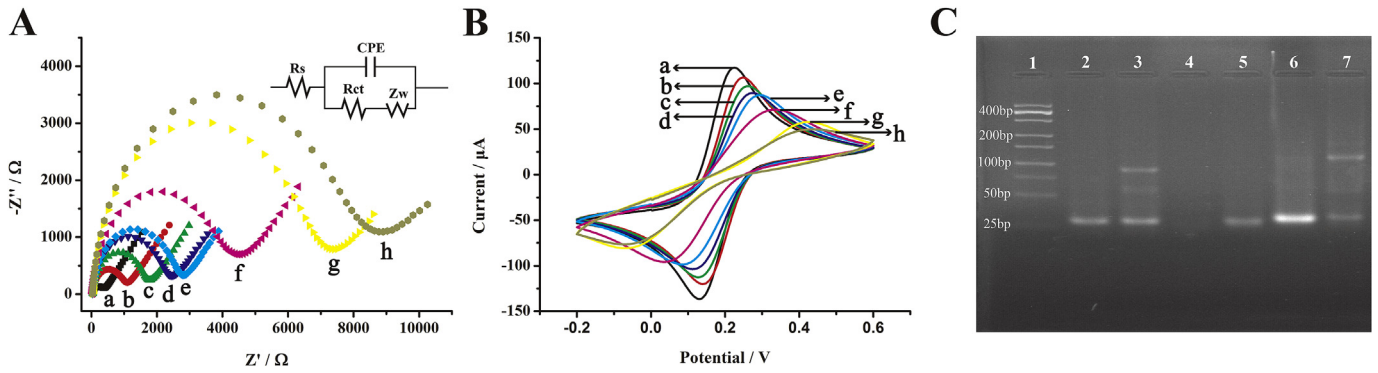

Fig. 1. Stepwise working electrode fabrication shown by the measurements of **(A)** EIS and **(B)** CV at a bare electrode (a), H5-modified electrode (b), MCH-modified electrode (c), BSA-modified electrode (d), after Exo III-CRA without (e) and with target DNA (f), after TDTase-CSA (g), and after interaction with streptavidin-alkaline phosphatase (h). Inset of panel A: the electrical equivalent circuit applied to fit the impedance data. Rct, Zw, Rs, and CPE represent charge transfer resistance, Warburg impedance, the Ohmic resistance of the electrolyte and constant phase element, respectively. **(C)** Agarose gel electrophoresis of Marker (lane 1), H1 + H2 (lane 2), target + H1 + H2 (line 3), target + H1 + H2 + Exo III (lane 4), H1 + H2 + Exo III (line 5), H3 + H4 + H5 (lane 6), target + H1 + H2 + Exo III + H3 + H4 + H5 (lane 7).

oligonucleotides facilitated the electrostatic repulsion of $[Fe(CN)_6]^{3-/4-}$, which indicated that H5 had been immobilized successfully on the surface of Au electrode. The semicircle diameter was further increased with an Rct value of about 1627 Ω (curve c) when MCH was immobilized on the electrode, which could be combined with the blocking effect of MCH to preclude electron permeation to the electrode surface. Afterwards, as the 1% BSA was added on the electrode, the semicircle diameter increased (curve d), the Rct value was about 2215 Ω. This effect was due to the biomacromolecules blocking the flow of electrons and increasing the resistance. When the assembled H5 reacted with amplification products of the exonuclease III-assisted cascaded recycling amplification (Exo III-CRA) without addition of the target DNA, the semicircle diameter was only slightly increased with a Rct value of about 2588 Ω (curve e). In contrast, after adding the target DNA, the semicircle diameter significantly increased (curve f) and the Rct value was rise to about 4443 Ω, indicating that only a trace amount of Y-shaped DNA nanostructures could be formed without target DNA participation; when target DNA existed, a large amount of Y-shaped DNA nanostructures were generated. After TDT-mediated cascaded signal amplification (TDT-CSA), the Rct obviously increased and the Rct value is about 6719 Ω (curve g), which proved that multiple biotin-11-dUTPs were successfully incorporated to extend the 3′-OH terminus of Y-shaped DNA. Then, via biotin-streptavidin interaction, multiple streptavidin-alkaline phosphatases were assembled on the surface of Au electrode, producing a large Rct of about 7969 Ω (curve h). As seen in Fig. 1B, the results obtained from CV measurements were consistent with the outcomes of EIS, where the peak currents varied with the stepwise assembly process. These results indicated that the biosensor indeed functioned as depicted in the working mechanism.

Additionally, we confirmed the proposed recycling process by using agarose gel electrophoresis. Agarose gel electrophoresis of Marker (lane 1), H1 + H2 (lane 2), target + H1 + H2 (line 3), target + H1 + H2 + Exo III (lane 4), H1 + H2 + Exo III (line 5), H3 + H4 + H5 (lane 6), and target + H1 + H2 + Exo III + H3 + H4 + H5 (lane 7) is presented in Fig. 1C. As exhibited in that figure, there is only one band in lane 2 at approximately 27 bps, suggesting that H1 and H2 cannot react with each other and that they can sufficiently maintain the stable stem-loop structure in solution. After adding target DNA, a new band with much lower mobility appeared, indicating that target DNA opened H1 and hybridized with H1, then the opened H1 can further open H2 to form a stable DNA duplex of T-H1-H2 (lane 3), and that this DNA duplex can be digested by Exo III (lane 4). Without target DNA, H1 and H2 cannot react with each other, and the Exo III cannot digest H1 and H2 (lane 5). With only H3, H4 and H5 present in the reaction mixture, there is only one band in lane 6 at approximately 29 bps, suggesting that H3, H4 and H5 cannot react with each other. After adding the amplification products of Exo III-CRA, a new band with much lower mobility appeared, suggesting that the amplification products of Exo III-CRA can open H5 and further form a Y-shaped DNA nanostructure (H3–H4–H5) just as recycle III described (lane 7). Thus, the agarose gel electrophoresis results demonstrated that each step of the recycling process was successful.

3.3. Feasibility of the proposed biosensor

The feasibility of the proposed biosensor for sensitive detection of target DNA was explored by performing DPV measurements. As exhibited in Fig. 3C, when the biosensors were utilized without target DNA (blank, curve a), there was only a small response signal. In the presence of target DNA (curve b), without the TDT-mediated cascaded signal amplification (TDT-CSA), nearly the same results as that obtained from blank (curve a) were observed because the ST-AP could not combine on the electrode surface. However, with TDT-mediated cascaded signal amplification for 30 min, the current intensity was obviously increased (curve c), demonstrating that biotin-11-dUTPs were successful added to the 3′-OH terminus of Y-shaped DNA. Curve d revealed that a more remarkable signal amplification had been achieved after 80 min, showing that the current was increased gradually with the extension of reaction time. This finding was clearly due to the elongation of multiple biotin-11-dUTPs to the 3′-OH terminus of Y-shaped DNA with time to produce two long biotin-11-dUTP tails, demonstrating that TDTase-CSA was successful.

3.4. Optimization of the experimental conditions

Experimental conditions play fundamental roles in the analytical performance. For obtaining the best analytical performance of the biosensor, some critical experimental conditions were chosen for investigation. In this work, the initial H5 amount strongly influenced the sensor performance. Therefore, the concentration of H5 was first evaluated. As presented in Fig. 2A, the current intensity increased as the H5 concentration increased until 0.5 μM. Later, the current intensity was reduced slightly with further increase in the H5 concentration, revealing that a high surface density of H5 could restrict SDR effectiveness because of the effects of steric hindrance. Thus, the best assembly concentration of H5 was 0.5 μM. The concentrations of H1 and H2 play important roles in the Exo III-CRA process. As shown in Fig. 2B, the current intensity increased with elevated H1 concentration until the H1 concentration reached 1.0 μM, at which point the current intensity reached saturation. Therefore, 1.0 μM was the optimized concentration

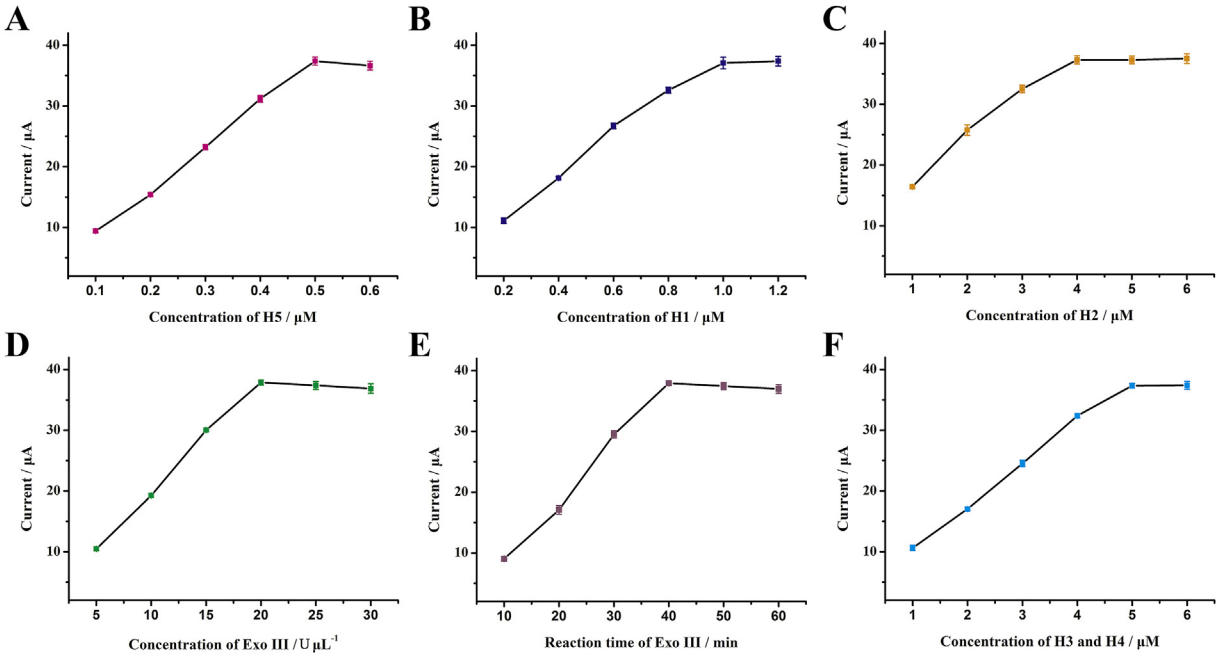

Fig. 2. Assessment of the effect of **(A)** H5 concentration, **(B)** H1 concentration, **(C)** H2 concentration, **(D)** Exo III concentration, **(E)** the reaction time of Exo III, and **(F)** H3 and H4 concentration. When one parameter changed, others were under their optimal conditions. The error bar stands for the standard deviation of three parallel measurements.

of H1. As Fig. 2C presented, the response signal was enhanced with increasing H2 concentration until the H2 concentration was 4 μM, when a plateau was reached. Therefore, the best concentration of H2 was 4 μM. The concentration of Exo III and the reaction time of Exo III could also influence the Exo III-CRA process. As Fig. 2D illustrated, the response signal increased until the concentration of Exo III exceeded 20 U/μL; therefore, the optimal concentration of Exo III was 20 U/μL. In the Exo III-CRA process, the reaction time of the Exo III represents another significant element that will affect the analysis performance of the biosensor. The current intensity increased as the reaction time of the Exo III-CRA progressed from 10 min to 40 min and then showed a tendency to decrease (Fig. 2E). Thus, 40 min was the optimal reaction time for Exo III.

The amount of H3 and H4 is a critical factor that influence the analysis performance of the biosensor. The impact of H3 and H4 concentration on the response signal was evaluated in the present study. As presented in Fig. 2F, the current intensity increased rapidly as the concentrations of H3 and H4 increased from 1 to 5 μM, and then, the corresponding signal reached a plateau. Therefore, the optimal concentrations of H3 and H4 were 5 μM. SDR reaction time, TDT concentration and TDT reaction time are also important for the experiment and were thus evaluated. The description of these optimization procedures are shown in Supplementary Material S3.

3.5. Analytical performance of the biosensor

For achieving the optimal analytical performance of the biosensor, the current responses toward target DNA at different concentrations were recorded under the optimal conditions to assess the analytical performance of this method through DPV measurements. As shown in Fig. 3A, the detection signal increased proportionally with increasing target DNA concentration in the 0.1 fM to 1 nM range. The corresponding calibration plots of the peak currents displayed a strong linear relationship to the logarithm value of target DNA concentrations in the detection range from 0.1 fM to 1 nM with a correlation coefficient of 0.9988 (Fig. 3B). The linear regression equation was I = 38.3758 + 4.0030 logC (I and C represent the peak current (μA) and the concentration of target DNA (nM), respectively). The detection

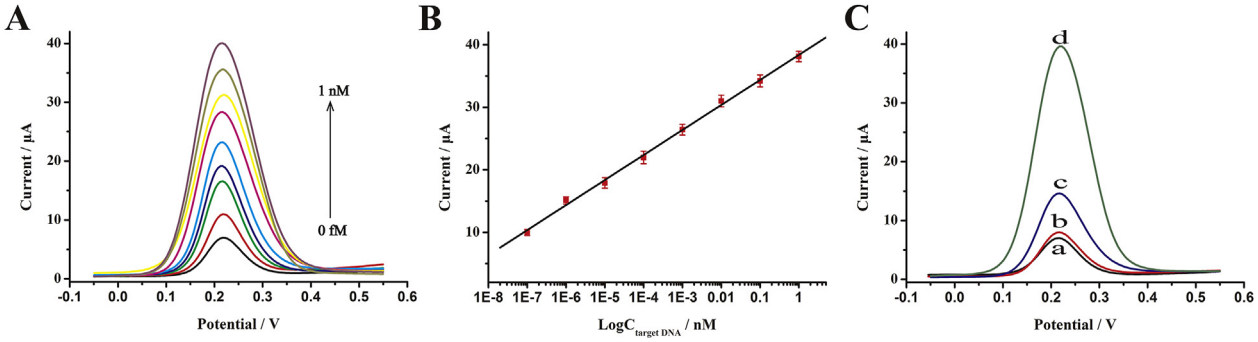

Fig. 3. (A) DPV curves response of the electrochemical biosensor upon the increase in target DNA concentration (from bottom to top: 0 fM, 0.1 fM, 1 fM, 10 fM, 100 fM, 1 pM, 10 pM, 100 pM, and 1 nM, separately). **(B)** Calibration curve of the DPV response versus the logarithm of target DNA concentration in the range from 0.1 fM to 1 nM. The error bar stands for the standard deviation of three parallel measurements. **(C)** DPV curves response of the electrochemical biosensor performed without target DNA (a); with target DNA, but without TDT-CSA (b); with target DNA and with TDTase-CSA for 30 min (c); and with target DNA and with TDT-CSA for 80 min (d).

limit was obtained based on three times the average standard deviation corresponding to the blank sample detection, which was as low as 0.05 fM. To our knowledge, the sensitivity of this proposed strategy for target DNA detection was better than most other amplified methods. Comparisons of this strategy with some reported methods are shown in Table S2. From the comparison, we can demonstrate that the proposed biosensor was better than other previously reported sensors regarding detection limit and linear range.

3.6. Specificity, repeatability and stability of the biosensor

The specificity of this experiment was evaluated by using the developed biosensor to detect five different DNA sequences, containing perfect complementary target DNA, single-base mismatched strand, inserted base strand, deleted base strand and random DNA sequence, all at concentrations of 1 nM. As depicted in Fig. S3 A, the response signals of none perfectly complementary sequences were nearly the same as the blank solution. However, in the presence of target DNA, the current response was remarkable increased (curve a). These results obviously indicated that the designed biosensor had a very high selectivity to DNA detection and offered potential application for DNA detection in real samples.

The fabrication reproducibility of the designed biosensor was investigated by measuring target DNA at three different concentrations: 10 fM, 1 pM, and 100 pM. As illustrated in Fig. S3 B, after five independent measurements, these electrodes exhibited similar current responses, and the relative standard deviations (RSD) for DNA detection were 2.12%, 3.18%, and 3.23%, respectively, indicating that the developed biosensor had a good fabrication reproducibility.

To evaluate the stability of the designed biosensor, the modified electrodes were stored in the refrigerator at 4 °C before use. As presented in Fig. S3 C, the experimental results demonstrated that the electrochemical signal of the biosensor retained approximately 95.09% of its initial electrochemical signal toward 1 nM target DNA after storage at 4 °C for 15 days. After storage for 30 days, the electrochemical signals retained 89.21% of the original magnitude, demonstrating the relatively robust stability of the developed biosensor.

All the results above suggested that the designed biosensor could effectively detect the target DNA with excellent selectivity, satisfactory reproducibility and acceptable stability.

3.7. Reusability of the biosensor

Reusability is a highly desirable feature for biosensor. The reusability of this biosensor was evaluated by detecting target DNA repeatedly using the proposed method. After one time of DNA detection, the electrode was simply kept in water at 90 °C for 5 min to dehybridization the double-stranded structure of the DNA on the electrode surface. Then, slowly cooled to ambient temperature to re-hybridization of nucleic acid strand to make a hairpin structure again. As a result, the electrode was return to the original assembled state, which could be used again for measurement. As shown in Fig. S4, after one detection, the electrode kept in water at 90 °C for 5 min, the electrochemical signal was almost the same as blank, it demonstrated that the architecture on the electrode surface was destroy. After five-repeated detection, the electrochemical signal was not significantly attenuated. Therefore, this biosensor could detect DNA accurately at least five times.

3.8. Application in clinical serum samples

To validate the application of the developed biosensor to practical complicated biological matrices, different concentrations of target DNA were added to 10-fold-diluted clinical serum samples and measured by DPV. The clinical serum samples were obtained from University-Town Hospital of Chongqing Medical University. The detection results of target DNA in human serum samples are summarized in Table S3. Satisfactory recovery values ranging from 94.98% to 105.36% were obtained, and the relative standard deviation (RSD) values were between 0.35% and 1.44%. These results confirm that the designed biosensor provides the possibility for clinical analysis.

4. Conclusions

In this work, an electrochemical biosensor for highly sensitive and specific DNA detection was achieved through isothermal cascade amplification. Compared to other DNA sensing strategies, this work utilized cascade signal amplification based on exonuclease III, strand displacement reaction and terminal deoxynucleotidyl transferase to obtain a detection limit as low as 0.05 fM. The developed biosensor presents a broad dynamic range from 0.1 fM to 1 nM, and does not require thermal cycling. The biosensor exhibits satisfactory reproducibility, acceptable stability and good reusability for DNA detection, is able to efficiently detect DNA in real human serum sample. The designed strategy is extensible to detect additional DNA by simply exchanging the relevant DNA sequence. Thus, the proposed electrochemical sensor shows a possibility for DNA detection in the fields of clinical molecular diagnosis, pathogen detection, gene therapy, food safety and environmental monitoring in the future.

CRediT authorship contribution statement

Xinyi Huang: Conceptualization, Data curation, Formal analysis, Writing - original draft, Writing - review & editing. **Wuceng Niu:** Conceptualization, Formal analysis. **Yang Wang:** Conceptualization, Formal analysis. **Chaorui Li:** Conceptualization, Formal analysis. **Jingfu Qiu:** Conceptualization, Formal analysis. **Jianjiang Xue:** Conceptualization, Formal analysis, Writing - review & editing.

Declaration of competing interest

The authors declare that they have no known competing financial interests or personal relationships that could have appeared to influence the work reported in this paper.

Acknowledgements

This research was supported by the National Natural Science Foundation of China (Grant Nos. 31071093, 31170129, and 31200064) and the Science and Technology Planning Project of Yuzhong District of Chongqing City, China (No. 20140119).

Appendix A. Supplementary data

Supplementary data to this article can be found online at https://doi.org/10.1016/j.bios.2019.111609.

References

Ahmed, A., Rushworth, J.V., Hirst, N.A., Millner, P.A., 2014. Clin. Microbiol. Rev. 27, 631–646.
Bi, S., Li, L., Cui, Y., 2012. Chem. Commun. 48, 1018–1020.
Bi, S., Yue, S., Wu, Q., Ye, J., 2016. Biosens. Bioelectron. 83, 281–286.
Chen, J., Liu, Z., Peng, H., Zheng, Y., Lin, Z., Liu, A., Chen, W., Lin, X., 2017a. Biosens. Bioelectron. 98, 345–349.
Chen, J., Wen, J., Yang, G., Zhou, S., 2015a. Chem. Commun. 51, 12373–12376.
Chen, J., Wen, J., Zhuang, L., Zhou, S., 2016. Nanoscale 8, 9791–9797.
Chen, J., Yu, C., Zhao, Y., Niu, Y., Zhang, L., Yu, Y., Wu, J., He, J., 2017b. Biosens. Bioelectron. 91, 892–899.
Chen, J., Zhou, S., Wen, J., 2015b. Angew. Chem., Int. Ed. Engl. 54, 446–450.
Chua, A., Yean, C.Y., Ravichandran, M., Lim, B., Lalitha, P., 2011. Biosens. Bioelectron. 26, 3825–3831.
Feng, Q.M., Guo, Y.H., Xu, J.J., Chen, H.Y., 2017. ACS Appl. Mater. Interfaces 9, 17638–17645.
Fern, J., Schulman, R., 2018. Nat. Commun. 9, 3766.
Ferrier, D.C., Shaver, M.P., Hands, P.J.W., 2015. Biosens. Bioelectron. 68, 798–810.
Hashsham, S.A., Wick, L.M., Rouillard, J.M., Gulari, E., Tiedje, J.M., 2004. Biosens.

Bioelectron. 20, 668–683.
Hsieh, K., Patterson, A., Ferguson, B., Plaxco, K., Soh, H., 2012. Angew. Chem., Int. Ed. Engl. 51, 4896–4900.
Huang, L., Zheng, L., Chen, Y., Xue, F., Cheng, L., Adeloju, S.B., Chen, W., 2015. Biosens. Bioelectron. 66, 431–437.
Hu, Y., Shen, Q., Li, W., Liu, Z., Nie, Z., Yao, S., 2015. Biosens. Bioelectron. 63, 331–338.
Li, F., Han, X., Liu, S., 2011. Biosens. Bioelectron. 26, 2619–2625.
Li, Z., Hayman, R.B., Walt, D.R., 2008. J. Am. Chem. Soc. 130, 12622–12623.
Lv, S., Zhang, K., Zeng, Y., Tang, D., 2018. Anal. Chem. 90, 7086–7093.
Mendoza, O., Mergny, J., Aimé, J., Elezgaray, J., 2016. Nano Lett. 16, 624–628.
Shen, Q., Han, L., Fan, G., Zhang, J., Jiang, L., Zhu, J., 2015. Anal. Chem. 87, 4949–4956.
Shi, K., Dou, B., Yang, J., Yuan, R., Xiang, Y., 2017. Biosens. Bioelectron. 87, 495–500.
Southern, E., 2006. Nat. Protoc. 1, 518–525.
Tadmor, A.D., Ottesen, E.A., Leadbetter, J.R., Phillips, R., 2011. Science 333, 58–62.
Wang, B., Wang, X., Wei, B., Huang, F., Yao, D., Liang, H., 2017a. Nanoscale 9, 2981–2985.
Wang, J., Wang, X., Wu, S., Che, R., Luo, P., Meng, C., 2017b. Biosens. Bioelectron. 87, 984–990.
Wang, P., Wan, Y., Deng, S., Yang, S., Su, Y., Fan, C., Aldalbahi, A., Zuo, X., 2016. Biosens. Bioelectron. 86, 536–541.
Woolley, A.T., Hadley, D., Landre, P., deMello, A.J., Mathies, R.A., Northrup, M.A., 1996. Anal. Chem. 68, 4081–4086.
Xuan, F., Fan, T., Hsing, I., 2015. ACS Nano 9, 5027–5033.
Yao, D., Song, T., Sun, X., Xiao, S., Huang, F., Liang, H., 2015. J. Am. Chem. Soc. 137, 14107–14113.
Zeng, R., Luo, Z., Su, L., Zhang, L., Tang, D., Niessner, R., Knopp, D., 2019a. Anal. Chem. 91, 2447–2454.
Zeng, R., Luo, Z., Zhang, L., Tang, D., 2018. Anal. Chem. 90, 12299–12306.
Zeng, R., Zhang, L., Luo, Z., Tang, D., 2019b. Anal. Chem. 91, 7835–7841.
Zeng, R., Zhang, L., Su, L., Luo, Z., Zhou, Q., Tang, D., 2019c. Biosens. Bioelectron. 133, 100–106.
Zhang, D., Hariadi, R., Choi, H., Winfree, E., 2013. Nat. Commun. 4, 1965.
Zhang, D., Seelig, G., 2011. Nat. Chem. 3, 103–113.
Zhang, K., Lv, S., Lin, Z., Li, M., Tang, D., 2018. Biosens. Bioelectron. 101, 159–166.
Zhang, Z., Luo, L., Chen, G., Ding, Y., Deng, D., Fan, C., 2014. Biosens. Bioelectron. 60, 161–166.
Zhou, Q., Lin, Y., Zhang, K., Li, M., Tang, D., 2018. Biosens. Bioelectron. 101, 146–152.
Zhu, L., Luo, L., Wang, Z., 2012. Biosens. Bioelectron. 35, 507–511.